Supporting Information

Sinha et al. 10.1073/pnas.1101818108

SI Note

Because our neuronal measurements can resolve single spH molecules, we often visualize distinct bleaching steps of surface spH in hippocampal neurons, which occur randomly during the time course of our optical recordings (0.5 s at 100 Hz) (Fig. S3). These bleaching steps are not stimulus locked (Fig. S3); their occurrence at any of the frames before or after stimulation, which are used to calculate the amplitude, can smear the noise peak toward the negative values (note that therefore in the noise peak of the distributions in Fig. 1*C*, even peaks or shoulders can be discerned corresponding to −1 or −2 pHl molecules). On the contrary, please note that the noise peak in our in vitro calibration experiments (Fig. 1*F*) does not suffer from this drawback (where locking in time is done with respect to a step-like bleaching event, not with respect to a stimulus) and therefore is a more reliable indicator of the true resolution in our measurements because the optical settings for both in vitro and in vivo measurements were identical.

SI Discussion

Optical recordings based on single-molecule photobleaching steps have been successfully used to precisely count membrane-bound proteins such as receptor subunits (1, 2), postsynaptic proteins (3), protein complex of bacterial flagellar motor (4), and very recently the multiprotein replisome complex of the active DNA replication machinery (5). The present study has applied such single-molecule fluorescence microscopy to determine the precise number of syb2 molecules sufficient to execute SNARE-dependent membrane fusion during fast synaptic transmission.

The finding that such a low copy number of syb2 can rescue evoked fusion raises concerns over the functionality of the chromophore. At first, the chromophore formation efficiency of GFP fusion proteins might affect the estimation of the functional spH molecules per SV. Previous studies have reported that the fraction of misfolding for GFP is very low and consequently the chromophore formation efficiency of GFP fusion proteins is very high—~80–90% (2, 3, 6)—too high to result in any underestimation in our measurements. An elegant study estimated this efficiency for postsynaptic GFP fusion proteins in hippocampal neurons (3). On the basis of anti-GFP immunostaining they suggested that ~70–80% of the fluorescent proteins are functional, which in this case represents a lower limit considering that not all of the epitopes can be bound by an antibody (3). To cause any appreciable underestimate of the SNARE molecules in our single-vesicle measurements and hence account for the lack of the single-molecule peak in Fig. 3*B* the folding efficiency has to be <10%.

The pHluorin moiety is attached to the ectodomain next to the transmembrane domain, which gives it ample time to fold during trafficking to the synapse. However, the folding of GFP should be fully independent of the SNARE motif structure on the other side of the membrane that might be still rather unstructured and might completely fold only when part of the SNARE complex. More importantly, we would expect the first molecular peak to be unaltered in the presence of misfolded nonfluorescent spH molecules contrary to Fig. 3*B*, because a fraction of the participating spH molecules in the SNARE complex would be always undetected. Thus, the fraction of nonfluorescent spH molecules could be well accounted for by the small remaining first nonzero peak of the intensity distribution for spH overexpression in DKO boutons (Fig. 3*B*).

Fast Ca^{2+}-triggered fusion in syb2-deficient hippocampal neurons is diminished >100-fold (7), and syb2 has been convincingly shown to be the only and predominant isoform of v-SNAREs in these synapses. Involvement of other v-SNAREs in our measurements can be excluded because of a near-complete reduction of Ca^{2+}-triggered exocytosis in the syb2 KO hippocampal neurons (7). Furthermore, previous studies have convincingly shown syb2 to be the only isoform expressed in these brain regions (7–9). Thus, we can clearly exclude that other v-SNARE/syb isoforms can compensate for the lack of syb2 by >1% in SV fusion. However, other noncognate SNARE interactions might occur, which could explain the residual (<1%) Ca^{2+}-triggered exocytosis in the above studies. In our data the dramatic reduction of the first molecular peak (Fig. 3*B*) is indicative of a clear and sole dependence on syb2 for evoked fusion.

SI Materials and Methods

Transgenes. Superecliptic pHluorin-synaptobrevin 2, SpH (10, 11), was kindly provided by G. Miesenböck (Yale University, New Haven, CT). Superecliptic pHluorin fused to synaptophysin 1, syp-pHl (12), was donated by Leon Lagnado (Medical Research Council, Cambridge, UK) and vGlut1-tagged pHluorin, vglut-pHl (13), was a gift from Robert Edwards (University of California, San Francisco). The fusion constructs syp-pHl and vglut-pHl were driven by CMV promoter whereas spH was driven by a neuron-specific human synapsin-1 gene promoter (11) and verified by dideoxynucleotide sequencing.

Optical Recordings. For single-vesicle optical measurements, single AP was applied at 0.15 s, and the sequence was repeated 10 times with an interval of 5–10 s in between consecutive trials. On average 10–20 boutons were imaged from one field of view on one coverslip due to the small chip size of the camera (DV-860 camera) used. For both WT and DKO spH single-vesicle recordings the data have been compiled from five to six independent transfections of hippocampal neurons prepared from eight to nine individual E18 pups that were later genotyped.

For single-vesicle recordings with spH-transfected boutons, imaged regions were prephotobleached for 50 s, using the same laser excitation (17 mW at back-focal plane) as during image acquisition. Fluorescence measurements of spH-expressing boutons for 40 APs and 100 APs were performed at reduced laser intensity (4 mW at back-focal plane) and at 2-Hz image acquisition frequency.

Bulk experiments (Fig. 2 *A–D* and Fig. S2) were performed with a 60×, 1.2 NA water-immersion objective. Images (512 × 512 pixels) were acquired with a back-illuminated EMCCD camera (DU-897E-BV; Andor Technology) controlled by Andor iQ Software (Andor Technology). PHluorin was excited at 488 nm with a computer-controlled monochromator (Polychrom IV; Till Photonics) and imaged using an eGFP filter set (AHF Analysentechnik AG). Time-lapse images were acquired at 0.2 and 0.5 Hz sampling frequency using an exposure time of 200 ms. Due to the larger chip size and lower magnification of the objective lens, >100 boutons could be detected per field of view for spH overexpression in WT and DKO neurons.

pHluorin Protein. The spH construct (11) was used as a template to introduce suitable 5′ and 3′ ends by PCR amplification for subsequent cloning into the pET21b(+) expression vector. A best clone screen was performed to identify the *Escherichia coli* clone with the highest protein expression. One hundred micrograms of

the pHluorin protein was purified and dissolved in 10 mM Tris, 10 mM EDTA (pH 8) with a final concentration of 1 μg/μL.

Image and Data Analysis. The difference image, generated by subtracting an average of five images in the time series before and after stimulation, was subjected to an à trous wavelet transformation with the level $k = 4$ and detection level $l_d = 1.0$, resulting in a segmented mask image (11). Spots on the mask image, each representing putative functional boutons, were identified, and their coordinates were used to overlay a square ROI of 1×1 μm on the original image series. Only masks with areas between 4 and 16 pixels were accepted for localizing the bouton fluorescence transients. All identified masks were visually inspected for correspondence to individual functional boutons. Mean fluorescence intensities from the ROIs were then plotted. ΔF was calculated as the difference in average intensity of five frames before and after stimulation (average peak fluorescence). Responses from all 10 trials of the experiments (including failures), for each detected bouton, were used to build the ΔF histograms in the case of spH. However, for amplitude distributions of vGlut-pHl and syp-pHl a fraction of the failures ($<1\ \sigma$ of the quantal size) was used to get a resulting noise peak in the histograms for fitting. Therefore, the vGlut-pHl and syp-pHl intensity histograms should not be used as a measure of release probability.

The ΔF histograms of single AP responses from spH, syp-pHl, and vGlut-pHl transfected boutons were fit to a multimodal Gaussian distribution constrained by the quantal size (width of each peak) q and coefficient of variation for the intensity measurements c_m on the basis of previously described procedures (14–16),

$$\sum_{k=0}^{n} A_k \cdot \exp\left(-\frac{1}{2}\frac{[x-(q\cdot k)]^2}{c_m^2\left[(q\cdot k+r)^2+r^2\right]}\right), \qquad \text{[S1]}$$

where A_k is the amplitude (number of responses) of the kth peak, q is the average intensity of an individual quantum (peak distance in the fit), c_m is the coefficient of variation of the quantal intensity, and r is the baseline/background fluorescence. The positions of each peak were constant and evenly spaced at integer multiples of q. Due to the smearing of the zero-order peak in the negative direction, only a subrange of the entire histogram was fitted as indicated by the overlaid best-fit curves. All Gaussian curve fitting were performed using Levenberg–Marquardt χ^2-minimization for nonlinear least-squares fitting. The baseline fluorescence r was taken as the average camera readout before stimulation and represents the background noise of our measurements that consists of a mixture of camera shot noise, laser-illumination noise, the signal from unquenched pHl-tagged molecules on the surface, and the quenched (1/25th) fluorescence of acidified SVs. This baseline fluorescence r determines the SD of the kth peaks. All other parameters were freely fit.

The in vitro single-molecule histograms were fit using a multi-Gaussian function,

$$\sum_{k=0}^{n} A_k \cdot \exp\left(-\frac{[x-\mu_k]^2}{2\sigma_k^2}\right), \qquad \text{[S2]}$$

where the parameters of the function, i.e., amplitude (A_k), peak spacing (μ_k), and SD (σ_k), are freely fit. Because the quantal size corresponds to single pHl molecules, the zero and first-order peaks in the in vitro experiments are comparable those of the single AP fluorescence responses and hence represent the true resolution of the optical measurements without any smearing in the negative direction of the zeroth peak as explained before. From these in vitro distributions we can derive the SD of the kth peaks on the basis of the following equation as previously described (14):

$$\sigma_{k\text{th peak}} = \sqrt{\sigma_0^2 + |k|\,\sigma_q^2}. \qquad \text{[S3]}$$

On the basis of the in vitro single-molecule distributions we could empirically determine σ_q and hence predict the SDs of the higher-order peaks in the single AP amplitude distributions (Fig. S6). The computed SDs were comparable to those estimated from the Gaussian fitting of individual higher-order peaks for the single AP spH distribution (Fig. S9). The SDs do increase with an increase in the mean ΔF amplitude as expected from Poisson statistics (Fig. S9), but this peak broadening is not very prominent because the baseline fluorescences r and σ_0 are relatively high and hence dominate the σ of the kth peaks. We circumvent this problem by averaging fluorescence intensity over five frames and over 16 pixels (4×4 pixels).

Lentiviral Transduction and Immunoblotting. The lentivirus plasmid expressing pHluorin fused to the C terminus of syb2 was used to infect hippocampal neuronal cultures at DIV 1. The neurons were lysed and harvested at DIV 12 using 0.1 mL of lysis buffer containing 150 mM NaCl, 10 mM Hepes (pH 7.4), 1 mM EGTA, 2 mM $MgCl_2$, 1% (vol/vol) Triton X-100, and a protease inhibitor mixture tablet (Roche, Applied Science). The lysates were centrifuged at 7,000 × *g* for 5 min. The supernatant was collected, denatured, and separated in 12% SDS/PAGE followed by Western blotting using standard procedures. The blot was probed with anti–Synaptobrevin-2, mouse monoclonal, clone 69.1 (1:6,000 dilution) (Synaptic Systems), followed by detection with an anti-mouse secondary antibody coupled to horseradish peroxidase. The blot was developed by enhanced chemiluminescence (PerkinElmer Life Sciences) and detected using a LAS 1000 CCD camera (Fugifilm). To show equal loading of each lane, the membranes were washed in stripping buffer, rinsed, and reprobed with polyclonal antibodies against lactate dehydrogenase (LDH) (SC-33781; Santa Cruz Biotechnology).

1. Haggie PM, Verkman AS (2008) Monomeric CFTR in plasma membranes in live cells revealed by single molecule fluorescence imaging. *J Biol Chem* 283:23510–23513.
2. Ulbrich MH, Isacoff EY (2007) Subunit counting in membrane-bound proteins. *Nat Methods* 4:319–321.
3. Sugiyama Y, Kawabata I, Sobue K, Okabe S (2005) Determination of absolute protein numbers in single synapses by a GFP-based calibration technique. *Nat Methods* 2: 677–684.
4. Leake MC, et al. (2006) Stoichiometry and turnover in single, functioning membrane protein complexes. *Nature* 443:355–358.
5. Reyes-Lamothe R, Sherratt DJ, Leake MC (2010) Stoichiometry and architecture of active DNA replication machinery in Escherichia coli. *Science* 328:498–501.
6. Patterson GH, Knobel SM, Sharif WD, Kain SR, Piston DW (1997) Use of the green fluorescent protein and its mutants in quantitative fluorescence microscopy. *Biophys J* 73:2782–2790.
7. Schoch S, et al. (2001) SNARE function analyzed in synaptobrevin/VAMP knockout mice. *Science* 294:1117–1122.
8. McMahon HT, et al. (1993) Cellubrevin is a ubiquitous tetanus-toxin substrate homologous to a putative synaptic vesicle fusion protein. *Nature* 364:346–349.
9. Trimble WS, Gray TS, Elferink LA, Wilson MC, Scheller RH (1990) Distinct patterns of expression of two VAMP genes within the rat brain. *J Neurosci* 10:1380–1387.
10. Miesenböck G, De Angelis DA, Rothman JE (1998) Visualizing secretion and synaptic transmission with pH-sensitive green fluorescent proteins. *Nature* 394:192–195.
11. Wienisch M, Klingauf J (2006) Vesicular proteins exocytosed and subsequently retrieved by compensatory endocytosis are nonidentical. *Nat Neurosci* 9:1019–1027.
12. Granseth B, Odermatt B, Royle SJ, Lagnado L (2006) Clathrin-mediated endocytosis is the dominant mechanism of vesicle retrieval at hippocampal synapses. *Neuron* 51: 773–786.
13. Balaji J, Ryan TA (2007) Single-vesicle imaging reveals that synaptic vesicle exocytosis and endocytosis are coupled by a single stochastic mode. *Proc Natl Acad Sci USA* 104: 20576–20581.
14. Gandhi SP, Stevens CF (2003) Three modes of synaptic vesicular recycling revealed by single-vesicle imaging. *Nature* 423:607–613.
15. Lemke EA, Klingauf J (2005) Single synaptic vesicle tracking in individual hippocampal boutons at rest and during synaptic activity. *J Neurosci* 25:11034–11044.
16. Murthy VN, Stevens CF (1998) Synaptic vesicles retain their identity through the endocytic cycle. *Nature* 392:497–501.

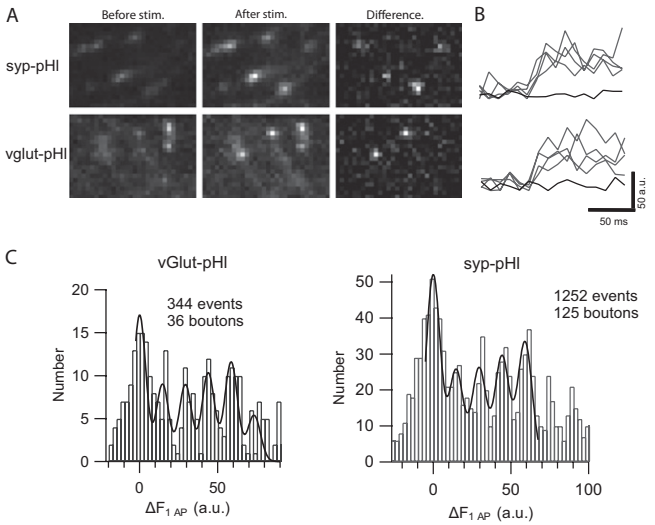

Fig. S1. Overexpression of vGlut-pHl or syp-pHl also exhibits quantal incorporation into SVs. (*A*) Image of syp-pHl and vGlut-pHl transfected boutons before and after stimulation. Difference image reveals sites of evoked release. (*B*) Exemplar fluorescence traces from individual boutons. (*C*) ΔF distributions from vGlut-pHl (*Left*) and syp-pHl (*Right*) overexpressing boutons evoked by 1 AP plotted with bin width of 2.5 a.u. The smooth solid curve is the best overall fit to multiple Gaussians (adjusted R^2 = 0.8 for both syp-pHl and vGlut-pHl). The unitary size determined by the function is 14.7 ± 0.17 a.u. for vGlut-pHl and 14.7 ± 0.15 a.u. for syp-pHl, equivalent to the single pHl molecule fluorescence in the gel (Fig. 1*F*).

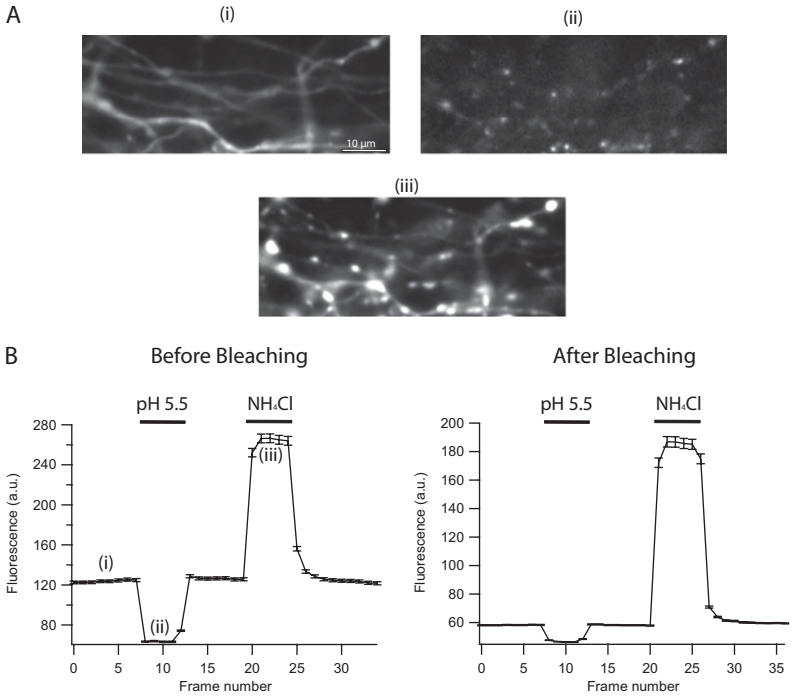

Fig. S2. Prebleaching selectively attenuates the surface-stranded spH without much affecting the vesicular spH fraction. (*A*) Fluorescence images of DKO neurons rescued with spH overexpression during the sequential pulses of an acidic solution and an ammonium chloride solution. (*B*) Exemplar average fluorescence traces before and after laser illumination for 50 s clearly show that ~90% of the surface spH molecules are photobleached and only ~10–15% of the vesicluar spH fraction is affected, consistent with the estimation from the single-molecule measurements (n > 1,000 boutons from four experiments). Error bars indicate SEM.

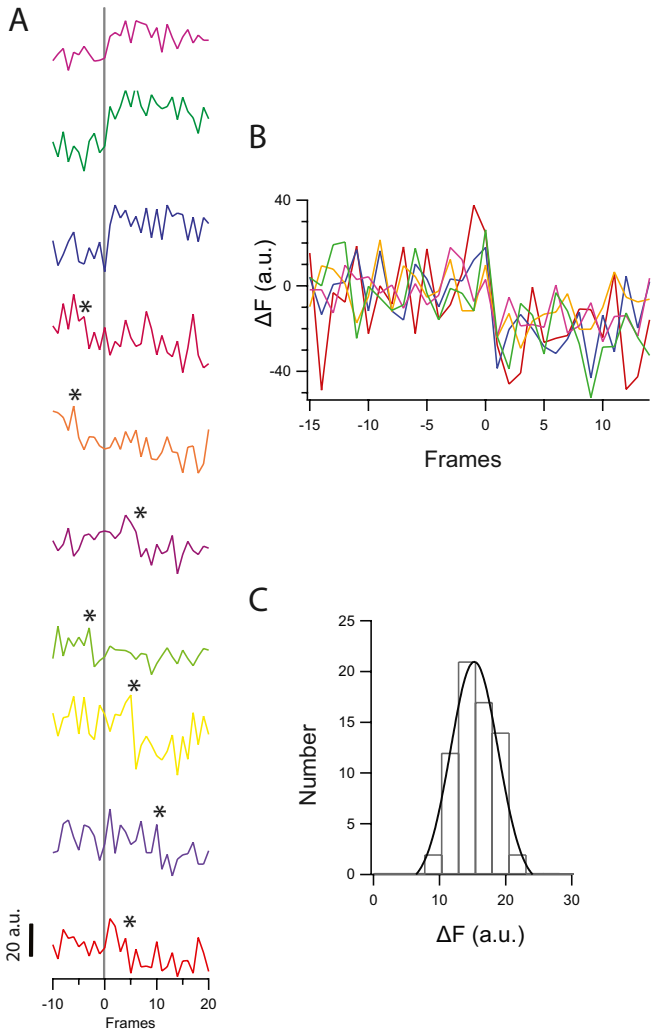

Fig. S3. Single-molecule fluorescence intensity quantified from bleaching steps in vivo. (*A*) Exemplar raw fluorescence traces indicating photobleaching steps occurring randomly (denoted by *) during the single-vesicle optical recordings not locked to the stimulation (gray bar) as opposed to first three evoked responses. (*B*) Photobleaching steps centered at the point of bleaching to quantitate the step size and hence single-molecule intensity. (*C*) Amplitude distribution (bin width 2.5 a.u.) of the fluorescence downsteps (n = 102) is well fit with a Gaussian curve denoted by the black line. The mean size estimated was 15.2 ± 0.29 a.u.

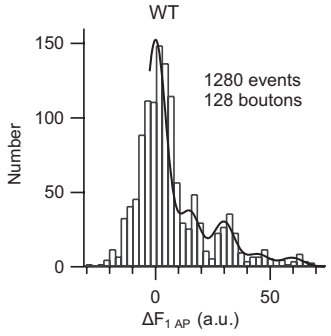

Fig. S4. Effect of increased prebleaching time on the relative frequencies of the molecular peaks in the histogram of spH-overexpressing WT boutons. Amplitude histogram is shown of responses evoked by 1 AP from spH-overexpressing WT boutons prebleached for 2 min. The histogram was plotted with 2.5 a.u. bin width and overlaid with the best-fit multiple Gaussian distribution (adjusted R^2 = 0.94). The unitary size estimated was 14.9 ± 0.67.

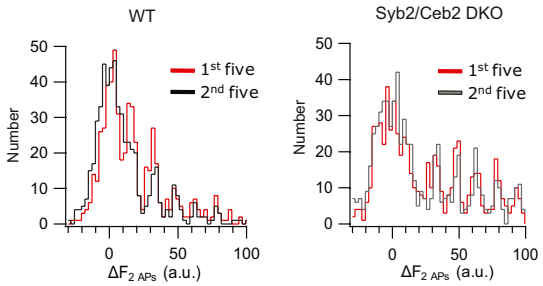

Fig. S5. Local reuse of readily releasable SVs does not occur during the measuring period of the experiment. The Δ*F* distributions from spH overexpressing WT (*Left*) and DKO boutons (*Right*) of the first five trials of the experiments were compared with the last five. The histograms were plotted with a bin width of 2.5 a.u. The peaks overlap and the relative amplitudes of the first to the second nonzero peaks are similar in both WT and DKO histograms.

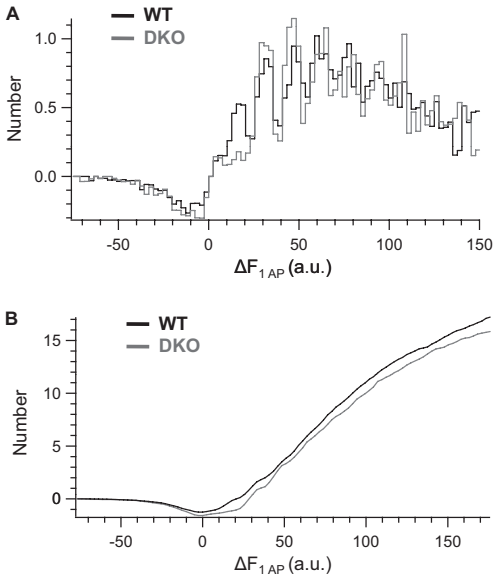

Fig. S6. Effect of missing first peak in DKO histograms on net fluorescence amplitude. (*A*) Intensity-weighted histograms generated by multiplying each bin by its respective bin width. The histogram was then normalized to the total number of events. The total sum of the histogram was calculated; i.e., WT = 34.41 a.u. and DKO = 31.69 a.u. Thus, there is a slight but negligible difference (<10%) between the WT and DKO histograms that is consistent with the amplitude histograms from the bulk stimulations (40, 100, and 900 APs). (*B*) This slight difference is better seen in the integrated histograms . Therefore, the missing first peak or failure of SVs, with 1 spH copy, to fuse does not affect the net fluorescence amplitude.

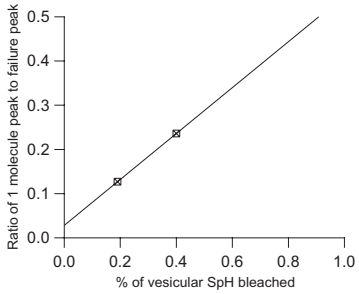

Fig. S7. Effect of prebleaching on the one-molecule peak. The ratio of the amplitude of the first molecular peak to that of the zeroth (failure) peak is plotted against the fraction of vesicular spH bleached calculated from the bleaching–waiting time plot in Fig. 1*G*. The two data points represent 50 s and 2 min prebleaching from Figs. 3*A* and 4*B*, respectively. The solid line is a linear fit with a *y*-intercept of 0.028, i.e., when there is zero bleaching.

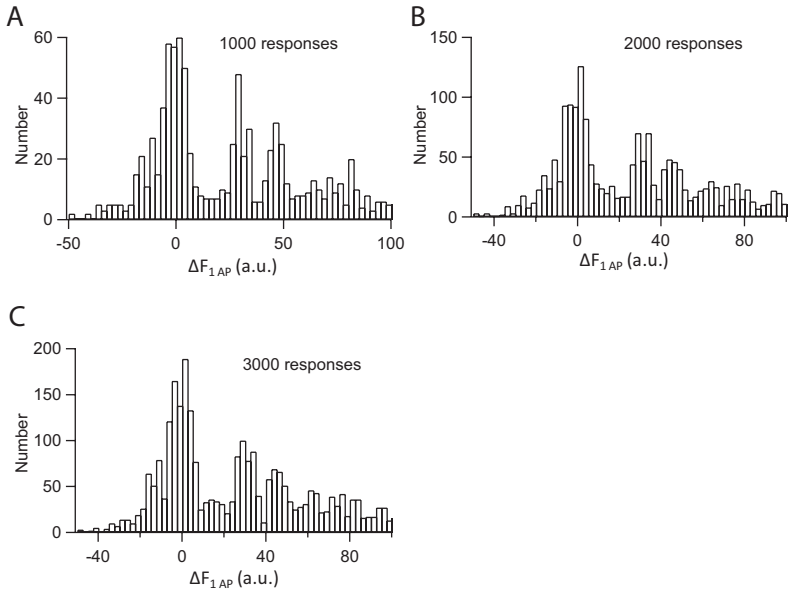

Fig. S8. Bootstrap analysis reveals sample size does not change the nature of the distribution in Fig. 3*B*. The entire data set from Fig. 3*B* was resampled using the StatsResample function in Igor Pro-6.03A. (*A*–*C*) Histograms of the first 1,000 values (*A*), the first 2,000 values (*B*), and the first 3,000 values (*C*) exhibit a marked reduction of the first nonzero peak as shown in Fig. 3*B*. Bin width is 2.5 a.u.

A

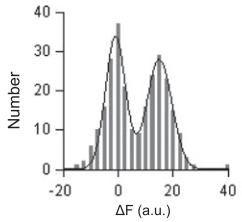

σ_0 = 5.15

σ_{k1} = 6.43

From eqn (iii) σ_q = 3.84

B

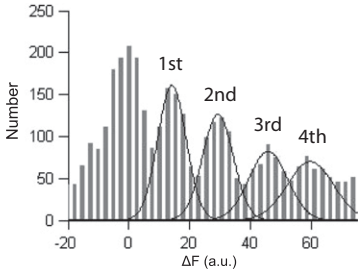

C

Peak no.(non-zero peaks)	Predicted σ_k from Fig (A)	σ_k from Gaussian fitting (Fig B)	μ_k from Gaussian fitting (Fig B)
1st	6.43	6.61	14.21 ± 1.05
2nd	7.48	7.15	29.35 ± 1.87
3rd	8.41	9.003	45.9 ± 1.67
4th	9.24	10.77	59.79 ± 2.1

Fig. S9. Comparison of SDs of ΔF distributions from single-moelcule and single-AP experiments. (*A*) Amplitude distribution of single-molecule bleaching steps from Fig. 1*F*. The quantal SD σ_q was estimated from Eq. *iii*. (*B*) Amplitude distribution of single AP fluorescence response from Fig. 1*C* fitted with individual Gaussian functions for each of the nonzero peaks. (*C*) Table comparing the calculated σ_k from *A* and Eq. *iii* with those predicted by *B*. There is a marginal increase in the σ_k values. The predicted μ_k values from *B* increase in multiples of the quantal fluorescence (mean of the first peak), i.e., 14.21 $\pm$ 1.05 units fully consistent with the multi-Gaussian estimates.